Supplementary Materials for

High Resolution Non-Contact Charge Density Mapping of Endocardial Activation

Andrew Grace[*], Stephan Willems, Christian Meyer, Atul Verma, Patrick Heck,
Lam Dang, Min Zhu, Xinwei Shi, Derrick Chou, Christoph Scharf,
Günter Scharf, Graydon Beatty

*Corresponding author. Email: aag1000@cam.ac.uk

This word file includes:

Materials and Methods

Fig S1. Workflow task for converting the trans-membrane potential to CD, for which CD is proportional to the spatial gradient of the transmembrane potential.

Fig S2. Illustration of evaluation metrics 'Xcorr' and Tdiff'.

Fig S3. Example of propagation history maps.

Fig S4. Illustration and calculation of ROC and AURC.

Fig S5. Example of D2O for simulated inferoseptal focal propagation.

Other Supplementary Material for this work includes the following:

Table S1 AcQMap Feasibility Criteria and Results

Movie S1 (mp4 format). Endocardial Surface Ultrasound Acquisition.

Movie S2 (mp4 format). Propagation History Maps of CD Versus Voltage.

Movie S3 (mp4 format). 'Typical 'Atrial Flutter in the Right Atrium.

Movie S4 (mp4 format). Individual Atrial Fibrillation Patterns – Focal.

Movie S5 (mp4 format). Individual Atrial Fibrillation Patterns – Localized Rotational Activation.

Movie S6 (mp4 format). Individual Atrial Fibrillation Patterns – Localized Irregular Activation.

Movie S7 (mp4 format). Individual Atrial Fibrillation Ablation Case Study.

Process Workflow and Output

1. Figure 2 illustrated the complete set of workflow tasks for each simulation. The first task was to simulate electrical propagation across the endocardial surface of the chamber.

2. Chaste software outputs transmembrane potentials to be used as an input to build *a priori* known distributions of CD. Figure S1 indicates the workflow of this conversion task. The spatial gradients of the transmembrane potentials, which define the depolarization wavefront, were calculated to represent the active, double-layer of charge-sources on the wavefront surface. Each gradient vector located at any given vertex was then converted to CD as a projected magnitude upon neighboring vertices aligned with the direction of the gradient vector. First, the vector was decomposed into two components aligned with the closest two triangle edges. Each component vector was then replaced by two discrete positive and negative charges (q_+ and q_-) positioned at each end of the triangle edge. The strength of each charge was set equal and satisfies the expression: $q = |q_+| = |q_-| = d/L$, where d is the magnitude of the vector and L is the edge-length. At the macroscopic level, these charges act as a continuous distribution of CD and were treated as the electric source for forward-calculating the surrounding potential-field.

3. The blood inside the chamber is an electrically homogeneous volume conductor that contains no sources. Cavitary potentials, $\phi(r)$, measured at any location, r, within the chamber are generated by the distribution of CD, ρ, contained within the surrounding myocardium and is governed by Poisson's equation:

$$\nabla^2\phi(r) = -\rho/r$$

The solution to Poisson's equation at any point in space for a known CD distribution on a surface can be expressed as the following surface integral (*85*):

$$\phi_i(r) = \frac{1}{4\pi\varepsilon}\int_S \frac{\rho(r')dr'}{|r-r'|} \qquad \textbf{(1)}$$

where $\phi_i(r)$ denotes the potential measured by electrode i at location r, while $\rho(r')$ denotes the CD at any location, r', on the endocardial surface S. ε denotes the electrical conductivity of the blood.

A prototype numerical implementation based on the boundary element method (BEM) was employed to compute the surface integral using a triangular mesh that represents the cardiac surface (*86*). Following the superposition principle, the CD source and measured potentials in equation **(1)** can be rewritten using the following linear matrix operation:

$$\phi = As \qquad \textbf{(2)}$$

where ϕ is a m×t matrix ('m' electrodes by 't' time instants) containing the measured potentials at the catheter electrodes, and s is an n×t matrix ('n' surface vertices by 't' time instants) containing the scalar values of CD on the chamber surface. A is the so-called m×n 'forward matrix' with elements representing the linear relationship between charge sources and the surrounding potential-field. Once the chamber surface vertices and catheter electrode positions were established, the forward matrix was computed and the 'ground-truth' potentials at the 48 electrodes were forward-calculated from the simulated CD using equation (**2**).

4. The AcQMap System inversely reconstructs CDs on the endocardial surface from the 48 measured potentials obtained from the AcQMap catheter. This inverse problem is underdetermined and sensitive to noise (ill-posed) so directly solving equation **(2)** is unstable. A methodology called 'regularization' was therefore applied to reduce sensitivity to noise and any type of input errors. Specifically, Tikhonov regularization (*4, 22*) was applied to solve the equation **(2)** as an optimization problem:

$$\min ||As - \phi||_2^2 + \lambda^2 ||s||_2^2 \qquad \textbf{(3)}$$

where $||\cdot||_2$ denotes ℓ_2-norm. The term of $||As - \emptyset||_2^2$ controls the data fitting error, while $||s||_2^2$ is the regularization term. λ is a constant, known as the regularization parameter, to balance those two terms. The solution of equation **(3)** is written as (*87*):

$$\hat{s} = A^T(AA^T + \lambda^2 I)^{-1}\phi \qquad \textbf{(4)}$$

where $\hat{s}$ is the estimated source and I is the identity matrix of size m×m.

Data Computation and Assembly

1. For each ‘run’ of simulated propagation, CD was inverse-reconstructed using equation (**4**). For mathematically practical reasons, all forward-calculations of potential on the chamber surface were performed with a small radial offset of 2 mm from each vertex toward the inside of the chamber and applied in equation (**2**). This small offset avoided the singularity (divide-by-zero) that prevents calculation directly on the vertex itself. For exact consistency, ground-truth potentials and forward-reconstructed potentials were both forward calculated from the simulated distributions and from the inverse-reconstructed distributions of CD, respectively, to the same radially offset locations

2. The instant at which a propagating wavefront reaches any specific point on the chamber surface is called ‘activation-time’ defined as the instant when the time-derivative of CD or potential reaches its peak-negative value throughout the duration of propagation at any specific location (*9*). Simulated CD was post-processed with this metric to establish the ‘actual’, ground-truth time-marker for local activation. Activation-time for inverse-reconstructed CD and forward-reconstructed voltages were identified using the AcQMap ‘timing-selection algorithm’, a spatiotemporal derivative that more accurately identifies the time of local activation than the time-derivative, by itself. However, in the specific case of the simulated CD, the time-derivative is equally accurate because the associated temporal waveform is free of noise and has an exceptionally ‘sharp’ morphology

Evaluation Metrics

1. Cross-correlation and Correlation Time-difference

In practical analysis and application, potential is expressed in units of Volts and, as such, the term voltage is synonymous and has been used in place of potential throughout. Ground-truth voltages were forward calculated from the simulated CD across the chamber surface (with 2 mm inward-radial offset) for comparison with forward-reconstructed values. All voltages were forward calculated for every instant over the duration of simulated propagation, resulting in a corresponding chamber-surface waveform that is equivalent to an intracardiac electrogram. Two hundred locations were randomly selected across the surface of the RA and LA bodies as points of comparison. Accordingly, cross-correlation was performed on the forward-reconstructed voltage-waveforms versus the ground-truth voltage-waveforms at all 200 random locations. All waveforms were normalized in amplitude and evaluated in terms of similarity of waveform morphology (Xcorr) and relative time-shift (Tdiff). Figure S2 illustrates the process required for the calculation of Xcorr by repeatedly shifting one waveform relative to the other from -50 ms to +50 ms, one sample per shift-step, and accumulating a set of Pearson correlation values for each shift-step. The Xcorr value was defined as the maximum of the set of correlation values. Tdiff was defined as the duration of time, in milliseconds, for the number of sample-shifts associated with the maximum correlation, as depicted in Figure S2.

2. **Area Under ROC Curve (AURC)**

The activation sequence can be characterized by a moving region of limited size upon the chamber surface that traces the path of wavefront conduction as a recent ‘history’ of propagation. This is constructed by accumulating and updating a moving window of activation-times during propagation of the wavefront. Such a propagation history map is displayed as a sequence of color-bands on the chamber surface. Figure S3 contains an example of a propagation history map from simulated ‘actual’ activation-times and ‘reconstructed’ activation times with a moving time window of 20 ms.

‘Binary’ maps were created by taking the entire region as a single, uniform representation of activation for both the actual and the reconstructed propagation history maps. From statistical detection theory, AURC was used to assess the sensitivity and specificity of the degree to which two spatial regions of propagation history equally overlap each other, as a binary classification (*88, 89*). This evaluation metric is illustrated and defined in Figure S4. The ROC curve is a graphical representation of the true-positive rate (also known as sensitivity) versus the false-positive rate (also known as 1-specificity). Results for which the curve trends close to the y-axis, vertically, and to the upper 100% line, horizontally, have high true-positive overlap of regions and low false-positive overlap. The AURC thus gives a quantitative measure of how similar the two spatial regions are in size, shape, and position over the entire duration of propagation (a spatiotemporal index of equality-of-overlap). AURC values range from 0.5 to 1.0, where 1.0 corresponds to a perfect match and 0.5 corresponds to a random match (Figures 3C, 3D).

3. **Spatiotemporal Correspondence between CD and Voltage**

AURC quantified the spatial accuracy of the reconstructed path of propagation as compared to the 'actual' path of propagation. Because AURC was calculated at each time frame, the distribution of AURC through time also provides a quantitative assessment of the temporal accuracy of reconstructed propagation. Temporal correspondence between CD and voltage was therefore also assessed by comparing propagation histories from inverse-reconstructed CD to the associated propagation histories from forward-reconstructed voltage.

4. **Distance to Origin**

Accuracy in localizing focal sites of propagation origin is a fundamental measure of performance of the resolution of 3D mapping and critically relevant to clinical practice. Reconstructed sites of early activation were characterized by the smallest-and-earliest emergence of a displayed zone of color on the propagation history map. To be classified as 'genuinely early', the associated instant of activation had to occur within 5 ms of the actual, known onset of simulated focal activation. For such color-zones that were classified as 'early', the specific site of origin was defined as the geometric center-point (centroid) of the zone. Distance-to-origin (D2O) was defined as the Euclidean distance, in millimeters, from the centroid of the identified zone of early activation to the actual, known location of simulated focal activation. This distance was established as a quantitative measure of spatial accuracy for the CD inverse algorithm. Figure S5 depicts an example of a D2O measurement on the inferoseptal region of the LA surface.

For the four evaluation-metrics defined above, acceptance criteria were established from the literature (*17, 18, 30*) and from the physicians' practical requirement to deliver a single clinically-relevant ablation lesion (5 mm diameter) to a specific target using an electrode catheter. This can be broken down as a spatial uncertainty of ≤ 5 mm in distance and a temporal uncertainty of ≤ 6 ms. Table S1 details the acceptance criteria for each objective measurement that demonstrates the mapping accuracy.

Supplemental Figures

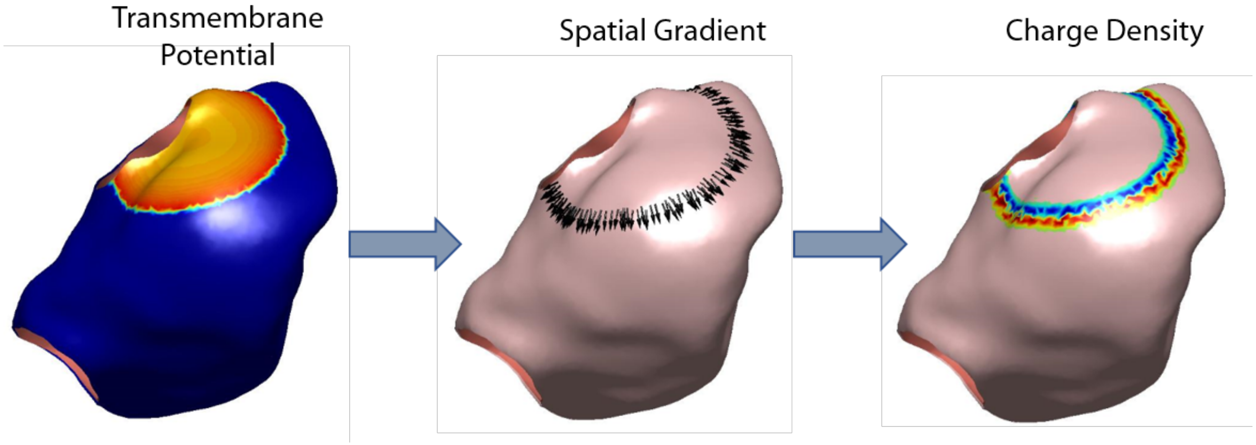

Figure S1: Workflow task for converting the transmembrane potential to CD, for which CD is proportional to the spatial gradient of the transmembrane potential.

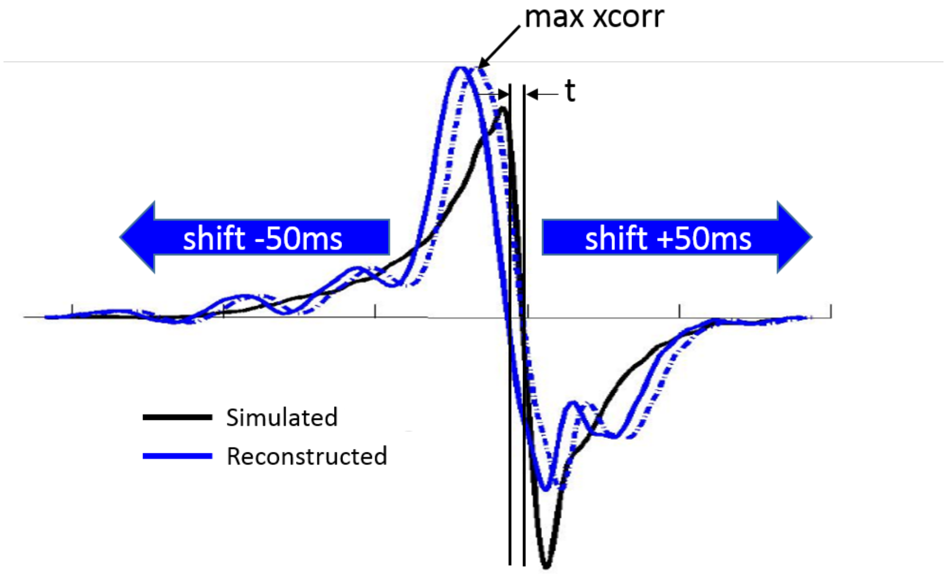

Figure S2: Illustration of evaluation metrics 'Xcorr' and Tdiff'.

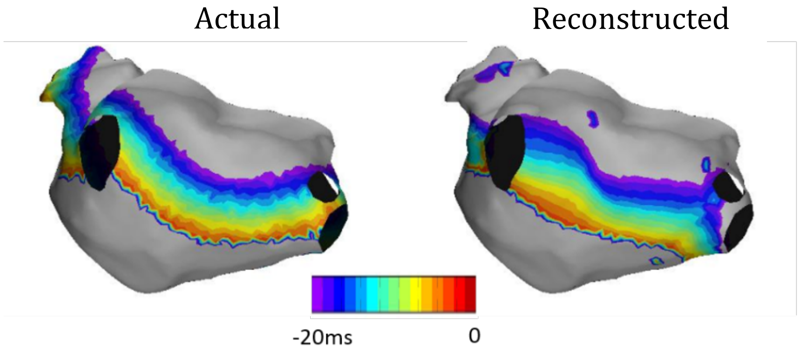

Figure S3: Example of propagation history maps.

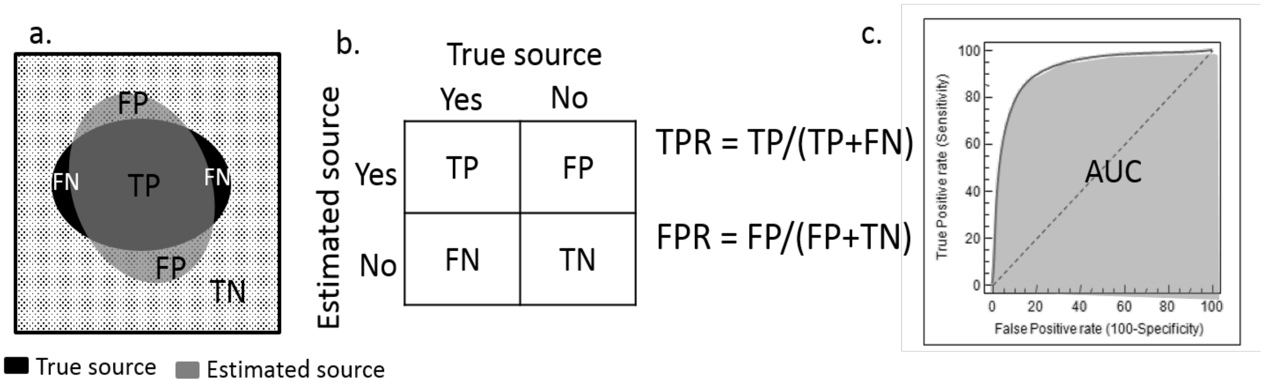

Figure. S4. Illustration and calculation of ROC and AURC. (a) Indication of true (black) and estimated (grey) source. (b) Contingency table and equations for true-positive rate (TPR) and false-positive rate (FPR). (c) ROC curve of FPR versus TPR.

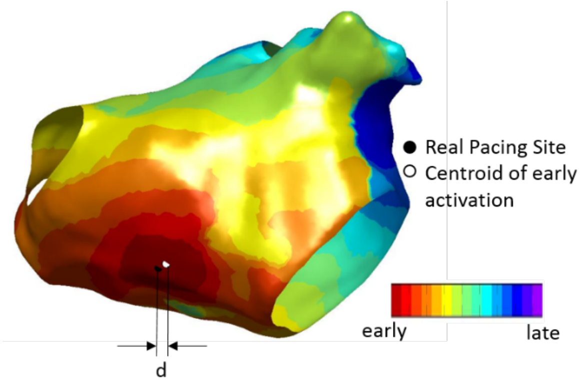

Figure S5. Example of D2O for simulated inferoseptal focal propagation. Activation-time derived from inverse-reconstructed CD was color-coded from early (dark red) to late (purple) activation. The white dot denotes the centroid of early activation identified for any instant <5 ms after the true onset of activation. The black dot denotes the actual site of simulated focal activation. The Euclidean distance, *d* (mm), measured between the two dots was recorded as D2O.

Table S1: AcQMap System Feasibility Criteria and Results

Parameter	Description	Assessment and outputs			
Map Accuracy: Voltage	Comparative analysis of a known/controlled/measured voltage on the surface to a calculated non-contact surface voltage over space and time.	30 sites of focal activation, 6000 sites of measurement	Xcorr of ground-truth surface voltage to forward-reconstructed surface voltage	Xcorr > 0.7 90% confidence	PASS
		30 sites of focal activation, 6000 sites of measurement	Tdiff of ground-truth surface voltage to forward-reconstructed surface voltage	Tdiff < 6 ms 90% confidence	PASS
		30 sites of focal activation, 6000 sites of measurement	AURC of Propagation History (20 ms window) of actual activation-times to Propagation History (20 ms window) of forward-reconstructed activation-times	AURC > 0.7 90% confidence	PASS
		30 sites of focal activation	D2O from actual focal site to forward-reconstructed site	D2O < 5 mm 90% confidence	83% †
Map Accuracy: CD	Comparative analysis of *a priori* known/controlled CD to an inverse-reconstructed surface CD over space and time.	30 sites of focal activation, 6000 sites of measurement	AURC of Propagation History (20 ms window) of actual activation-times to Propagation History (20 ms window) of inverse-reconstructed activation-times	AURC > 0.7 90% confidence	PASS
		30 sites of focal activation	D2O from actual focal site to inverse-reconstructed site	D2O < 5 mm 90% confidence	PASS
Map Accuracy: Charge/Voltage Correspondence	Comparative analysis of spatiotemporal correspondence between inverse-reconstructed CD and forward-reconstructed voltage	30 sites of focal activation, 6000 sites of measurement	AURC of Propagation History (20 ms window) of inverse-reconstructed activation-times to forwarded-reconstructed activation-times	AURC > 0.7 90% confidence	PASS

Notes:

† Due to the broad nature of voltage, the D2O metric met the < 5 mm criteria for 83% of the focal sites. The data is provided as a comparative verification of the performance of the prototype CD inverse algorithm. Importantly, CD and its inherent spatial specificity is the default mode of clinical operation for the AcQMap System in which all modes of diagnostic map displays are based.

Supplemental Movie Legends

Movie S1: Endocardial Surface Ultrasound Acquisition. The endocardial surface is sampled by the ultrasound sub-system at a rate of up to 115,000 surface points per minute and the 3D surface is algorithmically reconstructed from the ultrasound point-set in real time with distance acquisition based on the transit-time from transducer excitation to receipt of first sonic reflection. To scan the entire atrial surface anatomy, the catheter is slowly rotated within the deflectable guiding sheath, approximately 60 degrees clockwise and then counter-clockwise, while also advancing and retracting the catheter within the sheath throughout the chamber. Minimal editing is applied to achieve the final, CT-quality reconstructed anatomy, including removal of the mitral/tricuspid valve area and refinement of the vein structure as shown.

Movie S2: Propagation History Maps of Charge Density (CD) Versus Voltage. Both maps represent the rhythm pattern calculated from exactly one set of 'raw' input voltages recorded simultaneously from the AcQMap catheter. The resultant, derived CD map on the left shows a sharper, narrower, and localized irregular activation (LIA) pattern exhibiting multiple changes of direction through a discrete zone of interest (small yellow circle). The voltage-based map on the right was forward-calculated from the derived CD and it presents a broader, blended view of activation that is distributed across a large region and for which the localized zone of interest displayed by CD is obscured.

Movie S3: 'Typical 'Atrial Flutter in the Right Atrium. The map and waveforms reveal the activation sequence progressing inferiorly from the roof on the lateral wall (LAT), medially on the isthmus (CTI), and superiorly on the septum (SEP). Waveforms sampled from 8 evenly-spaced locations around the entire right atrium show the expected morphology and timing of propagation through the entire flutter cycle-length represented by the translucent-grey region.

Movie S4: Individual Atrial Fibrillation Patterns – Focal. Charge density map of a focal activation characterized by radial conduction from a single location ≥ 3 times per 5-second duration of AF.

Movie S5: Individual Atrial Fibrillation Patterns – Localized Rotational Activation. Charge Density map of localized rotational activation characterized by ≥ 270 degrees of conduction around a fixed, confined zone.

Movie S6: Individual Atrial Fibrillation Patterns – Localized Irregular Activation. Charge Density map of localized irregular activation characterized by repetitive, multidirectional entry, exit, and pivoting conduction through and around a fixed, confined zone.

Movie S7: Individual Atrial Fibrillation Ablation Case Study. The planned ablation strategy was to perform a conventional wide area encirclement of the left sided veins. The initial map of AF showed a single dominant localized irregular activation (LIA) in the posterior view that occasionally alternated into a rotational conduction pattern around the same site, the central point of which could be incorporated within a somewhat modified ablation line around the left pulmonary veins. The ablation strategy was modified to place contiguous lesions down the posterior wall with an approximately 1.5 cm wider encirclement than would be usual below the left inferior pulmonary vein to include the identified LIA.